Neuropathogenesis of Zika Virus in a Highly Susceptible Immunocompetent Mouse Model After Antibody Blockade of Type I Interferon

Darci R. Smith[1*], Bradley Hollidge[1], Sharon Daye[2], Xiankun Zeng[2], Candace Blancett[2], Kyle Kuszpit[3], Thomas Bocan[3], Jeff W. Koehler[4], Susan Coyne[4], Tim Minogue[4], Tara Kenny[3], Xiaoli Chi[3], Soojin Yim[2], Lynn Miller[5], Connie Schmaljohn[6], Sina Bavari[6] and Joseph W. Golden[1*]

[1]Department of Molecular Virology, Virology Division, [2]Pathology Division, [3]Molecular and Translational Sciences Division, [4]Diagnostics Systems Division, [5]Veterinary Medicine Division, [6]Headquarters Division, United States Army Medical Research Institute of Infectious Diseases, Fort Detrick, MD 21702

[*]Corresponding authors

E-mail: darci.r.smith.ctr@mail.mil and joseph.w.golden.ctr@mail.mil

Abstract

Animal models are needed to better understand the pathogenic mechanisms of Zika virus (ZIKV) and to evaluate candidate medical countermeasures. Adult mice infected with ZIKV develop a transient viremia, but do not demonstrate signs of morbidity or mortality. Mice deficient in type I or a combination of type I and type II interferon (IFN) responses are highly susceptible to ZIKV infection; however, the absence of a competent immune system limits their usefulness for studying medical countermeasures. Here we employ a murine model for ZIKV using wild-type C57BL/6 mice treated with an antibody to disrupt type I IFN signaling to study ZIKV pathogenesis. We observed 40% mortality in antibody treated mice exposed to ZIKV subcutaneously whereas mice exposed by intraperitoneal inoculation were highly susceptible incurring 100% mortality. Mice infected by both exposure routes experienced weight loss, high viremia, and severe neuropathology. The most significant histopathological findings occurred in the central nervous system where lesions represent an acute to subacute encephalitis/encephalomyelitis that is characterized by neuronal death, astrogliosis, microgliosis, scattered necrotic cellular debris, and inflammatory cell infiltrates. This model of ZIKV pathogenesis will be valuable for evaluating medical countermeasures and the pathogenic mechanisms of ZIKV because it allows immune responses to be elicited in immunologically competent mice with IFN I blockade only induced at the time of infection.

Author Summary

Research addressing the unexpectedly severe clinical complications associated with ZIKV infection, including Guillain-Barre (GBS) and congenital ZIKV syndrome, are urgently needed. Key to this effort is development of well-characterized animal models that recapitulate human

disease. Adult wild-type mice infected with ZIKV can develop viremia in some instances, but they do not emulate the disease associated with the severe congenital and adult neuropathology, which is occurring with the current ZIKV outbreak in the Americas. Several groups have recently described type I or type II IFN deficient murine models that are permissive for viral replication in several organs including the brain. The major limitation of these models is they utilize immunodeficient knockout mice that lack key components of the innate antiviral response. We describe the use of a lethal murine model for ZIKV in which the innate response of immunocompetent mice is suppressed only at the time of infection. We show that the mice develop severe neurological disease similar to that previously demonstrated in mice deficient in the type I or II IFN response. Using this model, we provide a detailed description of the ZIKV-associated pathology, much of which mirrors the neuropathogenic properties of ZIKV in humans. These studies will provide a baseline for assessment of medical countermeasures that can prevent or treat such pathogenic effects caused by ZIKV infection.

Introduction

Zika virus (ZIKV, *Flaviviridae*, *Flavivirus*) is an arthropod-borne virus (arbovirus) that is closely related to dengue, West Nile, Japanese encephalitis and yellow fever viruses [1,2]. ZIKV was first isolated in Uganda in 1947 from a febrile sentinel rhesus monkey in the Zika forest [3,4]. No significant outbreaks of ZIKV infection involving more than a few persons were detected until 2007, when ZIKV caused an explosive outbreak in Micronesia [5-8] where approximately 75% of the population on the island of Yap became infected during a four-month period [5]. In subsequent years, ZIKV continued to spread throughout Oceania [9-12]. In early 2015, ZIKV first emerged in the Western Hemisphere with an outbreak detected in Brazil

[13,14]. The virus spread rapidly throughout Latin America and the Caribbean and within one year most countries in the region reported local transmission [15,16]. ZIKV is expected to continue to spread and imported cases from travelers returning from Latin America and the Caribbean have already been reported in several countries including the U.S. and Europe [15,17-19]. In fact, numerous locally acquired mosquito-borne cases have recently been reported in Florida.

Historically, infection with ZIKV has been associated with a self-limiting febrile illness with no long-term sequelae, but more severe complications have become apparent during the recent outbreaks in the South Pacific and Latin America. In particular, significant concern is growing about the association of ZIKV infection and the development of fetal abnormalities such as microcephaly. ZIKV was isolated from the brains and cerebrospinal fluid of neonates born with microcephaly and identified in the placental tissue of mothers who had symptoms consistent with ZIKV infection during pregnancy [20-22]. An additional concern is the association of ZIKV infection and Guillain-Barré syndrome (GBS). GBS is an autoimmune polyradiculoneuropathy that can result in weakness, paralysis, and death [23-25], and was first associated with ZIKV infection during the 2013-2014 outbreak in French Polynesia. Cases of a diffuse demyelinating disorder consistent with GBS that are temporally associated with ZIKV infection have been reported in Brazil, El Salvador, Colombia, and Venezuela [26]. As ZIKV continues to spread, so does concern about the association of ZIKV infection and the development of severe clinical complications. Therefore, the development of medical countermeasures for ZIKV is a high research priority.

Animal models are needed to better understand the pathogenic mechanisms of ZIKV and to evaluate candidate medical countermeasures. Early ZIKV mouse models have relied on the

use of juvenile animals and/or intracerebral inoculations [3,4,27-35]. These initial studies suggest that in mice ZIKV can replicate and cause injury in cells of the CNS. In contrast, other animals to include cotton rats, guinea pigs, rabbits, and rhesus monkeys did not develop CNS disease even when infected by intracerebral inoculation [3]. In mice, neuronal degeneration and cellular infiltration were observed in regions of the spinal cord and brain [3]. Neuronal injury was also evident in the pathological evaluation of a human fetus infected *in utero* with ZIKV. Diffuse astrogliosis and activation of microglia were observed and damage extended to the brain stem and spinal cord [22]. Recently, mice deficient in the type I or type II interferon response were found to be highly susceptible to ZIKV infection [36-40]. ZIKV-infected *Ifnar1*$^{-/-}$ mice (C57BL/6 background mice lacking the IFN α/β receptor) developed severe neurological disease that was associated with high viral titers in the brain and spinal cord [39]. Similar results were described for A129 mice (129Sv/Ev background mice lacking the IFN α/β receptor), which were highly susceptible to ZIKV and developed neurological disease [36,38]. AG129 mice (129Sv/Ev background mice lacking the IFN α/β and γ receptors) were found to be more susceptible to ZIKV-induced disease compared to A129 mice [36]. Collectively, these efforts underscore the importance of innate immunity in modulating ZIKV infection and disease outcome.

The major limitation of these recently described ZIKV mouse models is that they utilize immunodeficient mice. These mouse models lack a key component of antiviral immunity which impairs comprehensive evaluation of medical countermeasures. In an attempt to produce infection models that do not rely upon knockout mice, several groups, including us, have explored the temporal blockade of IFN-I in immune intact mice using polyclonal and monoclonal antibodies targeting either IFN-Is directly or the IFN-I receptor [41-43]. A murine non-cell depleting monoclonal antibody (mAb) that efficiently targets the IFNAR-1 subunit of

the mouse IFN-α/β receptor (MAb-5A3) was recently developed and shown to prevent type I IFN-induced intracellular signaling *in vitro* and to inhibit antiviral, antimicrobial, and antitumor responses in mice [42]. MAb-5A3 has been used to explore the role of IFN-I in the infection and pathogenesis of several viruses including West Nile virus (WNV) [41], lymphocytic choriomeningitis virus, and vesicular stomatitis virus (VSV) [42]. For VSV and WNV, treatment of mice with this antibody results in a severe and lethal infection model similar to that produced in IFN-I receptor knockout mice. Here, we describe the use of MAb-5A3 antibody to block IFN-I signaling in immune intact, wild-type mice at the time of ZIKV infection. We demonstrate that these mice develop severe ZIKV-mediated disease accompanied by significant neuroinflammation and mortality when infected by multiple exposure routes. While we were completing this study, another group also reported the use of this system for ZIKV studies [39,44]. Although in the first report, these authors were unable to demonstrate ZIKV lethality, in the second study, they did find partial lethality using an African lineage strain that was derived from a brain homogenate by passage of the virus in *Rag1*$^{-/-}$ mice. Our report not only expands on those findings, but also provides the first comprehensive description of pathology associated with ZIKV infection using this model. This model of ZIKV pathogenesis will be valuable for evaluating medical countermeasures because it allows an immune response to be elicited in immunocompetent mice and infection is enhanced at the time of virus challenge.

Methods

Ethics statement. Research was conducted under an IACUC approved protocol in compliance with the Animal Welfare Act, PHS Policy, and other Federal statutes and regulations relating to animals and experiments involving animals. The facility where this research was conducted is

accredited by the Association for Assessment and Accreditation of Laboratory Animal Care, International and adheres to principles stated in the Guide for the Care and Use of Laboratory Animals, National Research Council, 2011.

Virus and pathogenesis study design. ZIKV strain DAK AR D 41525 isolated in 1984 from *Aedes africanus* mosquitoes in Senegal and was obtained from the World Reference Center for Emerging Viruses and Arboviruses (R. Tesh, University of Texas Medical Branch). It was amplified once in AP61 and C6/36 cells, and three times in Vero cells prior to use in this study and sequenced [45]. Female C57BL/6 mice (n=10/group; Jackson Laboratories) five weeks of age were injected IP with a total of 3.0 mg (2.0 mg first dose, 0.5 mg subsequent doses) of MAb-5A3 (produced by Leinco Technologies, St. Louis, MO) [42,46] or PBS on day -1, day +1, and day 4. On day 0, mice were infected with a target dose of 6 $\log_{10}$ PFU (actual dose was 6.4 $\log_{10}$ PFU) of ZIKV strain DAK AR D 41525 by the SC or IP exposure route. Mice were monitored for signs of disease and bled on day 4 post-infection (PI) or when euthanized to evaluate viremia.

qRT-PCR assay. Mouse serum samples were inactivated using a 3:1 ratio of TRIzol LS Reagent (Thermo Fisher Scientific, Waltham, MA). Tissues were homogenized in 1X Minimum Essential Medium with Earle's Salts and L-glutamine (MEM) with 1% penicillin/streptomycin and 5% heat-inactivated fetal bovine serum (FBS-HI) using a gentleMACS™ dissociator (Miltenyi Biotec, San Diego, CA) followed by centrifugation at 10,000 x g for 10 minutes and the supernatant was stored at -80°C until further evaluation. Supernatant was inactivated using a 3:1 ratio of TRIzol LS. Total nucleic acid from all samples was purified using the EZ1 Virus Mini Kit v 2.0 (Qiagen, Valencia, CA) and the EZ1 Advanced XL robot (Qiagen) according to the

manufacturer's recommendations. Samples were eluted in 60µL. Viral load was determined using a real-time RT-PCR assay specific to the 5'-untranslated region of ZIKV. Specific amplification detection was accomplished using a forward primer (5'-GARTCAGACTGCGACAGTTCGA), reverse primer (5'-CCAAATCCAAATTAAACCTGTTGA), and probe (5'-ACTGTTGTTAGCTCTCGC – MGBNFQ). A standard curve was generated using serial dilutions of the challenge virus having PFU/mL titers determined by plaque assay. Five µL of extracted nucleic acid were run in triplicate on the LightCycler 480 (Roche Diagnostics, Inc., Indianapolis, IN) using SuperScript One-Step RT-PCR (Thermo Fisher Scientific), and samples were considered negative if the cycle of quantification (Cq) was greater than 40 cycles. The virus titers were calculated using the standard curve and the LightCycler 480 software, and the final PFU equivalents/mL (PFUe/mL) calculations were determined based on the sample input volumes and the upfront sample dilutions.

Plaque assay. Vero cells were plated at $3x10^5$ cells/well in a six-well plate and incubated overnight at 37°C, 5% CO_2. Serial dilutions of samples were made in 1X MEM with 1% penicillin/streptomycin and 5% heat-inactivated FBS. Uninfected-control and serially-diluted samples were incubated with the Vero cells for one hour at 37°C, 5% CO_2 for virus adsorption. The inoculum was removed and a 1:1 mixture of 0.8% (w/v) Seaplaque agarose and 2X Basal Medium Eagle with Earle's Salts (EBME) solution containing 2X EBME, 10% FBS-HI, 2% penicillin/streptomycin, 50 µg/mL gentamicin, and 2.5 µg/mL Fungizone/Amphotericin B was added. After addition, the 0.4% Seaplaque agarose/2X EBME overlay was incubated at room temperature for 30 minutes to allow the overlay to solidify. Vero cells were incubated with the overlay at 37°C, 5% CO_2 for five days before the overlay was removed. Cells were fixed and

plaques were visualized by a 20 minute addition of 10% formalin with 50% Crystal Violet solution followed by a wash with water.

Histology. A necropsy was completed to collect the spleen, liver, head (to include brain), heart, kidney and spinal cord. All collected tissues were immersion fixed in 10% neutral buffered formalin for at least 2 days. The tissues were trimmed and processed according to standard protocols [47]. Histology sections were cut at 5 to 6 uM on a rotary microtome, mounted onto glass slides, and stained with hematoxylin and eosin (HE). Histological examination was performed by a board-certified veterinary pathologist.

ZIKV RNA *in situ* hybridization (ISH). *In situ* hybridization was performed using RNAscope® 2.5 HD RED kit according to the manufacturer's recommendations (Advanced Cell Diagnostics, Hayward, CA). Briefly, 20 ZZ probes set targeting the 1550-2456 fragment of the ZIKV polyprotein gene with Gene bank accession KJ776791.1 were synthesized. After deparaffinization and peroxidase blocking, the sections were heated in antigen retrieval buffer and then were digested by proteinase. The sections were covered with ISH probes and incubated at 40°C in a hybridization oven for two hours. They were rinsed and the ISH signal was amplified by applying Pre-amplifier and Amplifier conjugated with HRP. A red substrate-chromogen solution was applied for 10 minutes at room temperature. The slides were further stained with hematoxylin, air dried, and mounted.

Infrared and immunofluorescent imaging. Formalin-fixed, paraffin-embedded mouse brain sections on slides were deparaffinized in xyless and rehydrated through graded ethanol (100%, 95%, 90%, and 70%). Antigen was retrieved by citric acid-based antigen unmasking solution

(Vector Laboratories) during 10 minute boiling. After three washes with PBS (pH 7.4), the sections were blocked with 10% normal donkey serum in PBS-tween (0.1%; PBS-T) for one hour at room temperature. The sections were incubated with primary antibodies, goat anti-Iba1 (3 µl/mL; Novus Biotechnology) and Rabbit anti-GFAP (1:5000; Abcam), diluted in 10% normal donkey serum in PBS-T overnight at 4°C. After washing in PBS-T (3x5 min), the sections were incubated for 2 h at room temperature with secondary antibodies diluted in 10% normal donkey serum in PBS-T. For standard immunofluorescence, the secondary antibodies were donkey anti-goat Alexa Fluor 488 (1:300; Invitrogen) and donkey anti-rabbit Rhodamine-Red-X (1:200; Jackson ImmunoResearch). The nuclei were stained with Hoecht's. For infrared analysis, the secondary antibodies were donkey anti-goat IRDye 680RD (1:1500; Li-cor Biosciences) and donkey anti-rabbit IRDye 800CW (1:1500; Li-cor Biosciences). The sections were subsequently washed in PBS-T (3x10 min), PBS (3x5 min), and water (2x5 minutes). For immunofluorescence, the sections were coverslipped with Fluoromount-G (SouthernBiotechnology). For double-fluorescence labeling, primary rabbit anti-Zika Envelope (E) glycoprotein (1:400, IBT Bioservices) and mouse anti-alpha-Smooth Muscle Actin (1:200 Clone 1A4, R&D Systems) and secondary Alexa Fluor 488 conjugated goat anti-rabbit and Alexa Fluor 561 conjugated goat anti-mouse antibody were used. The nuclei were stained with 4′,6-diamidino-2-phenylindole (DAPI). Images were captured on a Zeiss LSM 780 confocal system and processed with Zen 2011 confocal, Photoshop, or ImageJ software. Sections for infrared analysis were air-dried overnight. A Licor-Odyssey CLx (Li-cor Biosciences) scanned sections at 21 µm/pixel resolution. The average intensities of GFAP and Iba1 on each slide were obtained from fields-of-interest draw around each section with the Li-cor-Odyssey analysis software on at least two sections per slide and three slides per brain were scanned. Negative

control staining, for which the primary antibodies were omitted, showed no detectable labeling in immunofluorescence or infrared imaging.

Statistical analysis. Survival analysis was completed by Kaplan Meier estimate. A one-way ANOVA by Kruskal-Wallis test with Dunn's multiple comparisons was used to analyze differences in viremia. A multiple t-test was used to compare tissue titers and an unpaired t-test was used to compare Iba1 and GFPA expression. SAS version 9.1.3 (SAS Institute Inc., Cary NC) was used for all analyses.

Results

ZIKV causes high mortality in immunocompetent mice when IFN-I signaling is blocked. Immunocompetent mice were treated with MAb-5A3 to block IFN-I signaling or PBS prior to and after challenge with 6 $\log_{10}$ PFU of ZIKV given by IP or SC injection. All of the PBS-treated mice challenged with ZIKV by either route survived and no apparent signs of disease, including weight loss were observed (Fig 1A and 1B). Mice exposed to ZIKV by the IP route and treated with MAb-5A3 began to succumb or were euthanized on day 7 PI at which time the mice presented with ruffled fur, hunched posture, and were poorly responsive. On day 8 PI, a mouse exposed SC and another mouse exposed IP exhibited right-side, hind-limb paralysis and were euthanized. Mice treated with MAb-5A3 and exposed to ZIKV by the IP route continued to succumb or were euthanized through day 12 PI where 100% (n=10/10) mortality was observed. MAb-5A3-treated mice challenged with ZIKV by the SC route continued to succumb through day 19 PI and resulted in 40% (n=4/10) mortality. The mean times-to-death (MTD) for mice exposed IP was 9.7 days and for mice exposed SC was 23.3 days, which were significantly

different (P<0.0001). Weight loss corresponded with survival for both challenge routes for mice treated with MAb-5A3. Mice treated with MAb-5A3 and exposed to ZIKV IP or SC began to lose weight on day 4 PI and 6 PI, respectively. Weight loss continued for MAb-5A3 treated mice exposed to ZIKV IP through day 12 PI when all mice had succumbed or were euthanized. MAb-5A3 treated mice exposed to ZIKV SC continued to lose weight until day 8 PI and then slowly began to regain weight and return to baseline values relative to day 0 PI by day 19 PI when mortality was no longer observed. These findings indicated that ZIKV can cause high mortality in mice with intact immune systems when IFN-I is blocked and that IP exposure was more lethal than SC exposure..

Viral titers in sera and tissues of ZIKV infected mice. The viral titers in the sera were determined on day 4 PI and when mice were euthanized (Fig 1C and 1D). All mice treated with MAb-5A3 and exposed to ZIKV developed viremia, however these levels were slightly (but not significantly) higher on average (0.6 $\log_{10}$ PFUe/mL higher) in IP exposed animals versus SC exposed animals. While all PBS-treated mice exposed to ZIKV by IP injection developed viremia, it was significantly ($p<0.0001$) lower on average (3.6 $\log_{10}$ PFUe/mL lower) compared to MAb-5A3-treated mice exposed to ZIKV IP. Most mice treated with PBS and exposed SC to ZIKV had viremia below the limit of detection for our assay (5/10), however, one mouse had a titer of >5 $\log_{10}$ PFUe/ml. There was no significant difference in the viremia of mice treated with PBS and exposed SC vs. IP. In addition to analyzing day 4 viremia in all mice, we also measured the viremia in animals succumbing to infection. At the time of euthanasia, viremia was generally lower compared to levels observed on day 4 PI. Moreover, we also examined the viral titers in the liver, spleen, heart, kidney, brain, and spinal cord when mice succumbed or were

euthanized (Fig 2). Virus was detected in all tissues collected and was generally higher in mice treated with MAb-5A3 and exposed IP to ZIKV. The only tissue with a statistically significant difference in titer for mice exposed IP vs. SC was the kidney ($p=0.01$). The highest amount of virus was detected in the spleen and brain of mice treated with antibody and exposed IP to ZIKV. These findings demonstrated that ZIKV infection in mice with IFN-I blockade results in high viremia and tissue titers. However, these mice were not perfused so some of the virus detected in the tissues may be from the blood.

ZIKV infection targets the CNS. We completed ISH and IFA coupled with histopathological analysis in tissues from ZIKV infected mice that succumbed or were euthanized due to severe disease. Significant histopathological changes occurred in the CNS of all ZIKV infected animals treated with the IFN-I blocking mAb-5A3 (Fig 3, S1 Table). The most notable microscopic lesions attributable to ZIKV infection in these mice included evidence of minimal to mild inflammation and necrosis in the brain and spinal cord of all animals that succumbed on days 7 and 8, and to a lesser extent, in at least 5 of the 9 animals that succumbed between days 11 and 19. The presence and /or extent of CNS lesions were difficult to ascertain in a few of the animals due to autolysis and/or artefactual damage to the tissue (S1 Table). Findings in the CNS included perivascular infiltrates of mononuclear cells (“perivascular cuffing") and multifocal to diffuse gliosis with activated microglia (Fig 3A). ZIKV RNA was frequently detected in the same regions by ISH (Fig 3B). Perivascular cuffing was a more consistent finding in mice that succumbed earlier (days 7-8) than in those that died or were euthanized later in the course of disease. In the sections examined, 5 of 5 animals from days 7 - 8, and 4 of 9 animals from days 11-19 exhibited perivascular cuffing in the brain; 4 of 4 animals from days 7- 8, but none from

days 11-19 exhibited perivascular cuffing in the spinal cord. In most animals, the perivascular cuffing was subtle, consisting of few mononuclear inflammatory cells; in 2 animals exposed to ZIKV IP that succumbed or were euthanized on day 7 PI, few neutrophils were admixed with the mononuclear cells. Microgliosis was a fairly consistent finding that was observed in the examined CNS sections of all animals from days 7 through 12. The severity was mild to occasionally moderate in animals that succumbed on days 7 - 8; whereas, microgliosis was minimal to occasionally mild in animals that succumbed on days 11 - 12.

Additional findings in the CNS included multifocal areas of neuropil vacuolation (edema) and scattered necrotic cellular debris, most notably in the cerebrum (Fig 3C), hippocampus (Fig 4A) and thalamus. Again, ZIKV RNA was detected by ISH in the same regions as these histopathological changes (Fig 3D and 4B). Multifocal areas of edema occurred in 5/5 animals from days 7-8, and in 3/6 animals from days 11-12. Tissue from animals that died on days 15, 17 and 19 were too autolyzed to accurately assess the presence of edema. Edema frequently surrounded blood vessels and was most prevalent in areas with the most abundant gliosis and neuronal necrosis. Scattered necrotic cellular debris often occurred adjacent to blood vessels and was observed in the brain of 5/5 animals from days 7-8, and in 5/6 animals from days 11-12. Although necrotic debris was often observed in multiple CNS sections, it was most frequently observed in the hippocampus, thalamus, cerebrum and less so in the cerebellum, pons and spinal cord. It is difficult to determine the cell type from which this necrotic debris originated—possibilities include neurons, resident glia, or infiltrating leukocytes.

An additional notable finding in the CNS was neuronal necrosis, characterized by hypereosinophilic neurons and pyknosis, karyolysis, and replacement of neurons with necrotic debris. Neuronal necrosis occurred most frequently and extensively in the hippocampal

pyramidal and granule layers and less frequently in the thalamus, cerebrum, and least frequently in the cerebellum, pons and spinal cord (Fig 4C). Once again, RNA was consistently detected in corresponding regions of the brain by ISH (Fig 4D). In the sections examined, neuronal necrosis was observed in the brain of 4/5 animals from days 7-8 and 3/4 animals from day 11, and 0 animals from days 12-19; however, autolysis of the tissue precluded adequate evaluation of several of the animals that succumbed at the later time points. Neuronal necrosis was also observed in the spinal cord of 4/4 animals examined from days 7-8 and 2/2 animals examined from day 11, while no neuronal necrosis was observed in the spinal cords of animals from days 12-19; however, autolysis of the tissue precluded adequate evaluation of several of the animals that succumbed at the later time points. Less frequently there was neuronal degeneration and satellitosis. Another, although less consistent finding, was minimal neutrophilic infiltrates scattered within the brain parenchyma, which was observed in only 2/5 animals from days 7-8, and 3/9 animals from days 11-19.

Histopathological analysis of the spinal cord showed evidence of one or more of the following: gliosis, neuronal satellitosis, and perivascular inflammatory infiltrates, in all mice observed (Fig 5A). The detection of ZIKV RNA by ISH in the spinal cord suggests that these lesions are also due to infection (Fig 5C). In general, cells in the spinal cord were only occasionally observed to be positive for ZIKV RNA by ISH; however, in some animals the spinal cord was more severely affected, and massive ZIKV infection was detected by ISH in some animals as depicted in Fig 5C. Additionally, a focally extensive area of necrosis affecting a spinal ganglion was observed in a mouse exposed to ZIKV IP that succumbed on day 7 PI (Fig 5D).

It has been known that both ionized calcium binding adaptor molecule 1 (Iba1) expressed by microglia and glial fibrillary acidic protein (GFAP) expressed by astrocytes are upregulated in activated microglia and astrocytes, respectively, during neuroinflammation [48,49]. Infrared and immunofluorescent imaging was used to assess the effect of ZIKV on neuroinflammation by detecting the expression of Iba1 and GFAP in brain sections from 10 of the mice that succumbed to ZIKV infection (brains from four of the mice were not analyzed due to artifactual damage). Compared to brains of control mice treated with IFNAR1-blocking MAb-5A3, Iba1 and GFAP levels were significantly increased in the brains of ZIKV-infected mice (Fig 6A-B) and these findings were confirmed by immunofluorescent labeling of Iba1 and GFAP in these brains (Fig 6C). Collectively, the results suggest that in our model, CNS infection by ZIKV results in significant neuroinflammation.

Additional pathology induced by ZIKV Infection. Other significant findings outside of the CNS include necrotic and/or apoptotic cellular debris within the splenic lymphoid follicles (white pulp) interpreted as lymphocytolysis (Fig 7A). This was a fairly consistent finding in these mice, with similar lesions being observed in all (8/8) spleens examined (S1 Table). The severity of the lymphocytolysis varied from mild in the earliest stages (3/3 animals from day 7) to minimal in all subsequent animals. Additionally, several animals (2 from day 7, 1 from day 8 and 1 from day 11) exhibited minimal lymphoid hyperplasia in the spleen, presumably in response to ZIKV infection. ZIKV RNA was also consistently detected by ISH in cells in the white pulp of the spleens from these animals (Fig 7B). No significant histopathological findings were observed in the liver, kidney, and heart; however, ISH staining was observed in the smooth muscle cells within the tunica media of blood vessels in the kidney and heart (Fig 7C). IFA

confirmed the presence of ZIKV in the smooth muscle of blood vessels in the kidney (Fig 7D). The lack of concurrent microscopic evidence of tissue injury despite the presence of ZIKV in these mice suggests that, although virus is present in the smooth muscle, no direct damage to these cells is occurring; however, further studies are needed to fully elucidate the significance of ZIKV presence in smooth muscle of these blood vessels. Also, it is unclear why ZIKV appears to be present in the tunica media of vessels of these two organs but not in other organs examined.

Additional findings of interest outside the CNS include the observation of degeneration, inflammation, and less consistently, regeneration, of skeletal muscles of the head and vertebral column. Myocyte degeneration, inflammation, and nuclear rowing were evident by hematoxylin and eosin staining (Fig 8A-B). However, ZIKV was not detected in the skeletal muscle by ISH. Inflammation and degeneration was a fairly common finding, and was noted in at least one anatomic site from all 14 animals examined. Regeneration was observed less frequently, with minimal regeneration occurring in 8 animals. Although lesions were observed in skeletal muscles from multiple anatomic sites, no similar lesions were observed in cardiac muscle. The skeletal muscle observed in this study was limited to the head and vertebral column regions. Future investigations should include examination of the skeletal muscles from the rear limbs, particularly since hind limb paralysis was observed in two of the mice.

Inflammatory infiltrates were observed in the vitreous chamber of the eye in three mice that succumbed to ZIKV infection (Fig 8C-D). ZIKV RNA by ISH was detected in ganglion cells and/or cells in the inner nuclear layer of the eye in the same percentage of mice, but these results did not always correlate with the histologic findings. Ocular abnormalities and ZIKV ISH signal detection was only observed concurrently in a single mouse. It is unclear if these inflammatory infiltrates represent a virus-associated lesion since ISH did not consistently detect

ZIKV RNA and there was no evidence of damage to ocular tissues associated with these minimal infiltrates.

Discussion

The unexpectedly frequent and severe clinical complications of ZIKV infection, including GBS and congenital ZIKV syndrome, have prompted intense research on host-virus interactions. Such studies have been hampered by the absence of reliable and well-characterized animal models that mimic the viral pathogenesis in humans. Adult wild-type mice infected with ZIKV can develop viremia in some instances [50], but do not reflect the severe neurological disease seen in humans. Knockout mice, deficient in type I or type II IFN responses, are permissive for viral replication in several organs including the brain [36-40]; however, infection in these mice does not provide an adequate means to test the efficacy of medical countermeasures or to study pathogenic events after infection. For example, in addition to its role in controlling viral infection through antiviral gene induction, type I IFN plays a role in priming of B and T cell responses [reviewed in [51,52]. Therefore, a more immunologically competent mouse model is essential for evaluating vaccines and treatments for ZIKV.

We developed and characterized an immunocompetent murine model of ZIKV infection replicating the pathology noted in genetically modified mice through antibody blockade of the type I IFN receptor. We are using this model to evaluate vaccines and therapeutics and as reported herein, have used the model to establish a baseline of ZIKV pathogenesis. As we were completing our pathogenesis study, another group reported a similar model. In their initial study, a non-lethal model of ZIKV infection was described in wild-type mice injected IP with 1 mg or 2 mg of the same IFN-1 blocking antibody that we used and then exposed SC to 3 $\log_{10}$ focus-

forming units of ZIKV strain H/PF/2013, which is a human isolate from the 2013 French Polynesia outbreak [39]. ZIKV replication was observed in several organs of mice treated with the antibody; however, the mice did not lose weight, succumb to infection, or develop neuropathology. In their second report, IFN blockade by the same monoclonal antibody followed by SC infection with a higher dose of an African lineage strain of ZIKV (Dakar 41519) that was derived from a brain homogenate via passage in *Rag1*$^{-/-}$ mice resulted in lethal disease [44]. Our mouse model results are similar to those in this second report in that we found that antibody blockade of the type I IFN receptor recapitulates the severity of ZIKV disease observed in *Ifnar1*$^{-/-}$ mice. Further, we demonstrated that route of exposure is a factor in lethality in this mouse model in that mice exposed by the IP route began to succumb on day 7 PI and 100% mortality was observed by day 12 PI. In contrast, 40% mortality was observed when mice were exposed SC and they succumbed as late as day 19 PI. However, the disease was similar in mice that succumbed to ZIKV regardless of the route of exposure where severe pathology was observed in the CNS. Zhao et al. report higher lethality by SC infection which may be due in part to passaging their virus in mice [44]. Our results and those described by Zhao et al. suggest that the virus strain (African vs. Asian lineage), passage history, and exposure route can affect susceptibility to infection. More studies are needed to evaluate the pathogenesis of African vs. Asian lineage strains (and the effect of passage history) in the various infection models.

Mortality is not a common feature of human infection with ZIKV, which is generally asymptomatic and self-limiting in most individuals. However, severe disease in humans is characterized by neurological complications associated with ZIKV infection. In adults, reported neurological complications include GBS [24,25] or in a few cases, encephalopathy [53], meningoencephalitis [54], and acute myelitis [55] have been described. In the fetus, intrauterine

infection can cause congenital abnormalities to include severe fetal brain injury [22]. The neuropathology that we observed in our studies offers a model for dissecting the pathological consequences of ZIKV infection. We observed severe pathology in the CNS of all mice that succumbed to ZIKV infection. Overall, the CNS lesions in these mice represent an acute to subacute encephalitis/encephalomyelitis that is characterized by neuronal death, astrogliosis, microgliosis, scattered necrotic cellular debris, and a minimal to mild mononuclear (and less frequently neutrophilic) inflammatory cell infiltrate. In the brain, lesions were most evident in the hippocampus, particularly affecting the pyramidal and granule cell layers, followed by thalamus and cerebrum, and less often affecting the cerebellum and pons. The presence of ZIKV RNA as detected via ISH suggests these lesions are attributable to ZIKV infection. It is likely that encephalitis/encephalomyelitis contributed to the morbidity and mortality in these animals, particularly those that succumbed early, between days 7 to 11. Lesions, particularly neuronal necrosis and inflammation, appear to be less severe in animals from day 12; however, it is possible that CNS injury played a role in the deaths of these animals as well. The neurotropism of ZIKV was demonstrated in early studies where neonatal mice intracerebrally infected with ZIKV showed evidence of nuclear fragmentation, perivascular cuffing, and degenerative cells in the hippocampus of the brain [3,28]. Bell et al. also observed enlarged astrocytes with extended processes and containing cytoplasmic virus factories throughout the cortex of ZIKV infected mouse brains [28]. More recent studies characterizing ZIKV murine models in immunodeficient mice also showed that microscopic lesions resulting from ZIKV infection were found primarily in the brain [37,38,40]. Our findings are most consistent with those reported by Dowall et al. [38] where inflammatory and degenerative changes were observed in the brains of A129 mice challenged with ZIKV. The CNS lesions observed in ZIKV infected mice may be relevant for

brain-related pathologies in some ZIKV-infected humans. However, the histopathology of ZIKV-associated microcephaly has been limited to only a few reports thus far (reviewed in [56]). The major findings have mostly been in the brain and include diffuse grey and white matter involvement consisting of dystrophic calcifications, gliosis, microglial nodules, neuronophagia, and scattered lymphocytes [56]. Astrocyte pathology was observed in post-mortem analysis of a neonatal brain with microcephaly associated with ZIKV infection where diffuse astrogliosis was apparent with focal astrocytic outburst into the subarachnoid space. Activated microglial cells were also found to be present throughout most of the cerebral gray and white matter [22].

Outside of the CNS, the most consistent histopathological lesions were observed in the spleen. We observed lymphocytolysis in the splenic white pulp which correspond to areas with ZIKV ISH signal. Dowall et al. also noted similar lesions in the spleen although detection of viral RNA was not described [38]. Other histopathological observations indicated a significant inflammatory response resulting from ZIKV infection. Lymphoid hyperplasia and myeloid (granulocytic) hyperplasia were noted and are indicative of an inflammatory response to antigenic stimulation and an increased demand for leukocytes. Although these are both somewhat non-specific findings, in these cases they most likely represent a systemic immune reaction to ZIKV infection and are related to the significant neuroinflammation noted in the animals. A previous study indicated that ZIKV infection in AG129 mice led to a systemic inflammatory response, where multiple pro-inflammatory cytokines were found to be increased in the sera [40]. It is unknown how this relates to human disease since the cytokine response during the acute phase of ZIKV infection in humans has not been studied.

Inflammation was also observed in the skeletal muscles of the head and vertebral column. Skeletal muscle degeneration and inflammation observed in these animals are thought to be

attributable to ZIKV infection; however, no ZIKV RNA was detected in skeletal muscle sections by ISH. Interestingly, Ailota et al. described similar pathology in the musculature from the posterior rear limb of a ZIKV infected mouse where multi-focal myofiber degeneration and necrosis with inflammatory cell infiltration, nuclear rowing, and attempted regeneration were observed. Because it is unclear if these lesions represent direct infection of myocytes by ZIKV, or a secondary, possibly immune-mediated injury, further investigation may be warranted.

The role of ZIKV in the inflammatory infiltrates observed in the eyes of 3 of the animals is also unclear. Although ISH detected the presence of ZIKV RNA in retinal ganglion cells and/or cells of the inner nuclear layer in 3 animals as well, only one animal exhibited concurrent microscopic findings of vitreous chamber inflammatory infiltrates and retinal ZIKV RNA, which further confounds the association. Additional studies may be beneficial in elucidating any correlations; however, this finding is of interest because ocular complications have been described in ZIKV infected humans [57]. Interestingly, a recent study in mice demonstrates that ZIKV can infect different regions of the eye to include the iris, cornea, retina, and optic nerve leading to conjunctivitis, panuveitis, and neuroretinitis [58].

In summary, we described a murine model for ZIKV that mimics the severe neurological disease previously described in mice deficient in the type I or II IFN response [37,38,40]. Our detailed description of the ZIKV-associated pathology in this model, much of which mirrors what is known about neuropathogenesis in humans, will provide a baseline for evaluating medical countermeasures to prevent or treat ZIKV infections.

Author Contributions

Conceptualization, J.W.G, D.R.S, B.H.; K.K, T.B., S.D., L.M.; Methodology, D.R.S, J.W.G, B.H.; J.W.K, S.C, T.M, X.Z., S.D.; Investigation, D.R.S, B.H., J.W.G, J.W.K, S.C., X.Z, S.D. ;

Resources, T.K., X.C.; Writing—Original Draft, D.R.S, B.H. ; Writing—Reviewing & Editing, D.R.S., J.W.G, B.H., S.D, T.B., L.M., C.S, S.B.; Supervision, C.S., S.B.

Acknowledgements

We would like to thank Andrew Haddow, Farooq Nasar, and Veronica Soloveva for providing the virus stocks used in this study, Sam Washington for statistical support, Nichole Roberts for animal technical support, and Chris Kane and Robert Lowen for programmatic support. We would also like to thank Dr. Stephen Lockett and Kimberly Peifley at Optical Microscopy and Analysis lab at NCI-Frederick for assistance with confocal imaging. Opinions, interpretations, conclusions, and recommendations are those of the author and are not necessarily endorsed by the U.S. Army.

Funding disclosure

This work was supported by DARPA.

Supplemental Table. Significant Microscopic Findings in ZIKV Infected Mice Treated with an IFNAR1-Blocking mAb.

	Animal #	M1/IP	M2/ IP	M3/ IP	M4/ IP	M1/ SC	M5/ IP	M6/ IP	M7/ IP	M8/ IP	M9/ IP	M10/ IP	M2/ SC	M3/ SC	M4/ SC
	Day PI	7	7	7	8	8	11	11	11	11	12	12	15	17	19
	Comments	FD	E	E	E	E	FD	E	E	E	E	E	FD	FD	FD
Organ	Lesion														
Brain	Perivascular cuffing	2	1	2	1	2	0	0	1	0	0	1	1	0	1
Brain	Microgliosis	2	2	2	2	2	1	1	2	1	1	1	0	0	0
Brain	Neuronal necrosis	1	2	1	3	0	0	1	3	1	0	0	0	0	0
Brain	Scattered necrotic debris	1	1	2	2	2	0	1	1	1	1	1	0	0	0
Brain	Neutrophilic infiltrates	1	0	0	1	0	0	1	0	1	1	0	0	0	0
Brain	Neuropil vacuolation (edema)	2	1	1	1	1	0	1	1	0	0	0	0	0	0
Spinal cord	Perivascular cuffing	1	1	1	n/a	2	n/a	n/a	0	0	0	0	0	0	0
Spinal cord	Microgliosis	3	2	1	n/a	2	n/a	n/a	1	1	0	1	0	0	0
Spinal cord	Satellitosis	0	1	0	n/a	1	n/a	n/a	0	1	0	0	0	0	0
Spinal cord	Neuronal necrosis	1	1	1	n/a	1	n/a	n/a	1	1	0	0	0	0	0
Spinal cord	Neuropil Vacuolation (edema)	2	1	1	n/a	2	n/a	n/a	1	1	0	0	0	0	0
Spinal ganglion	Necrosis	2	0	0	n/a	0	n/a	n/a	0	0	0	0	0	0	0
Spleen	Lymphocytolysis	2	2	2	1	1	n/a	n/a	1	1	n/a	1	n/a	n/a	n/a
Spleen	Lymphoid hyperplasia	1	1	0	0	1	n/a	n/a	1	0	n/a	0	n/a	n/a	n/a
Skeletal muscle, head	Inflammation	0	1	0	2	1	1	1	1	1	0	0	0	1	1
Skeletal muscle, head	Degeneration	0	1	0	1	1	2	1	1	1	0	0	0	1	0
Skeletal muscle, head	Regeneration	0	0	0	1	0	0	1	1	1	0	0	0	0	0
Skeletal muscle, vertebral	Inflammation	2	1	1	n/a	2	2	3	1	2	1	1	1	1	1
Skeletal muscle, vertebral	Degeneration	1	1	1	n/a	1	2	1	1	1	1	1	1	1	0
Skeletal muscle, vertebral	Regeneration	0	1	0	n/a	0	0	1	0	1	1	1	1	0	0
Eye, vitreous chamber	Inflammatory cell infiltrates	0	0	0	2	1	0	1	0	0	0	0	0	n/a	n/a
Bone marrow	Myeloid hyperplasia	3	2	3	n/a	2	1	0	2	2	2	2	2	2	n/a
Liver	Hepatic lipidosis	3	3	3	3	2	n/a	1	0	0	0	0	0	0	0
Score:	0= none 1=minimal, 2=mild, 3=moderate, 4=marked, 5=severe														
	Artefactual damage and/or autolysis precludes adequate assessment of tissue														
	SC route of challenge														

Figure Legends

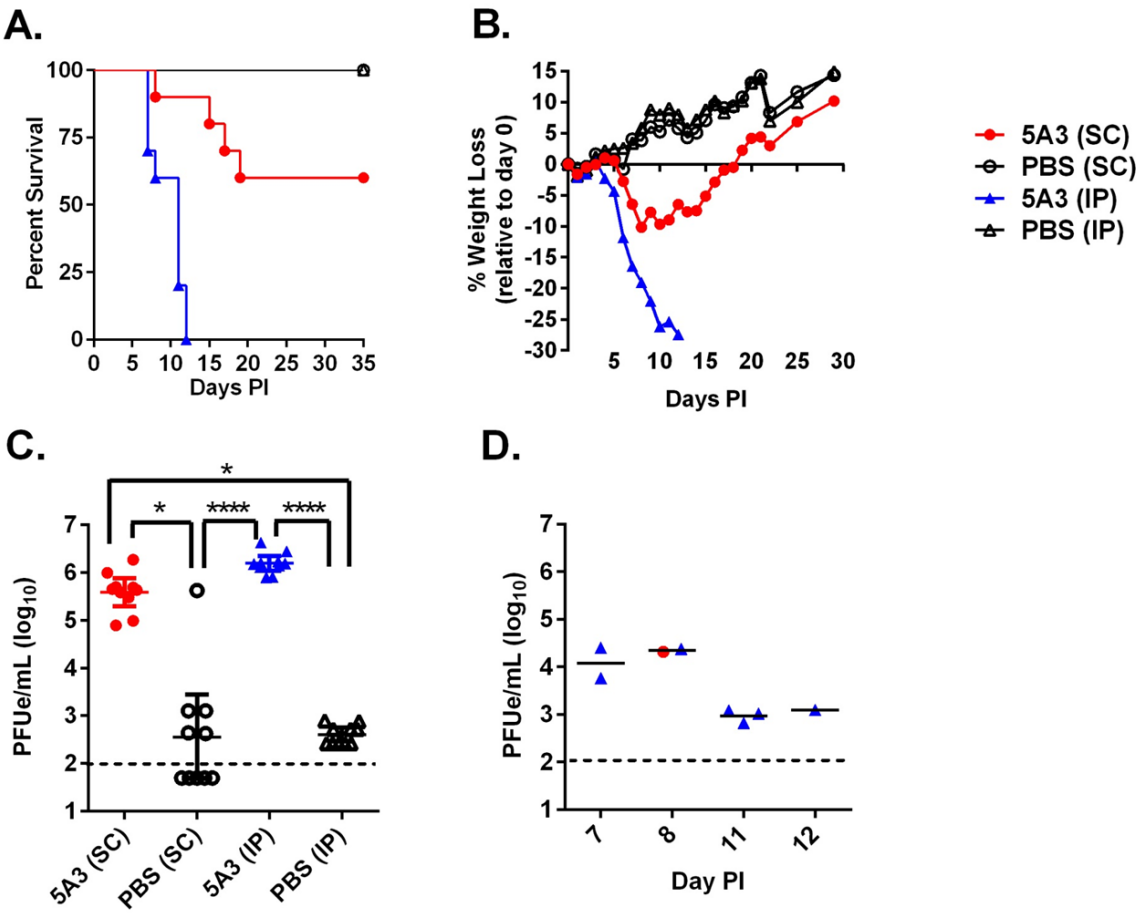

Fig 1. WT Mice Treated with an IFNAR1-Blocking mAb are Susceptible to ZIKV. Five week old WT mice were treated with an IFNAR1-blocking mAb or PBS by IP injection and then exposed to 6 $\log_{10}$ of ZIKV strain DAK AR D 41525 SC or IP. Mice were monitored for survival (A) and weight loss shown as percent change in baseline prior to infection (B). ZIKV RNA in serum was determined on day 4 PI (C) and when the mice were euthanized (D) by qRT-PCR. Data are shown as PFU equivalents (PFUe) per milliliter after normalization to a standard curve. Symbols represent the individual mice and the line represents the geometric mean. The dotted line represents the assay limit of detection. Statistically significant differences are denoted by an asterisk (*$p < 0.05$; *$p < 0.0001$).

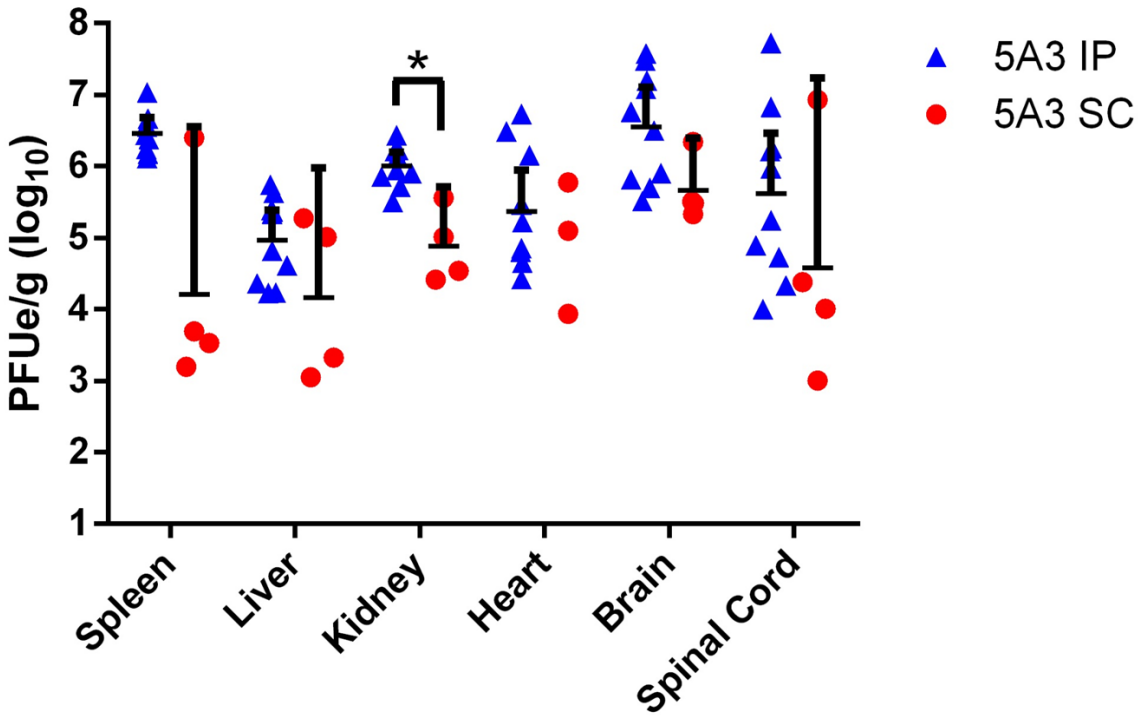

Fig 2. Viral titers of ZIKV in WT Mice Treated with an IFNAR1-Blocking mAb. Five week old WT mice were treated with an IFNAR1-blocking mAb or PBS by IP injection and then exposed to 6 $\log_{10}$ of ZIKV strain Dak ArD 41525 SC or IP. When mice succumbed or were euthanized, tissues were collected, weighed, homogenized, and analyzed by qRT-PCR. Data are shown as PFUe per gram (g) after normalization to a standard curve. Symbols represent the individual mice and the line represents the geometric mean. Statistically significant differences are denoted by an asterisk (*$p < 0.05$).

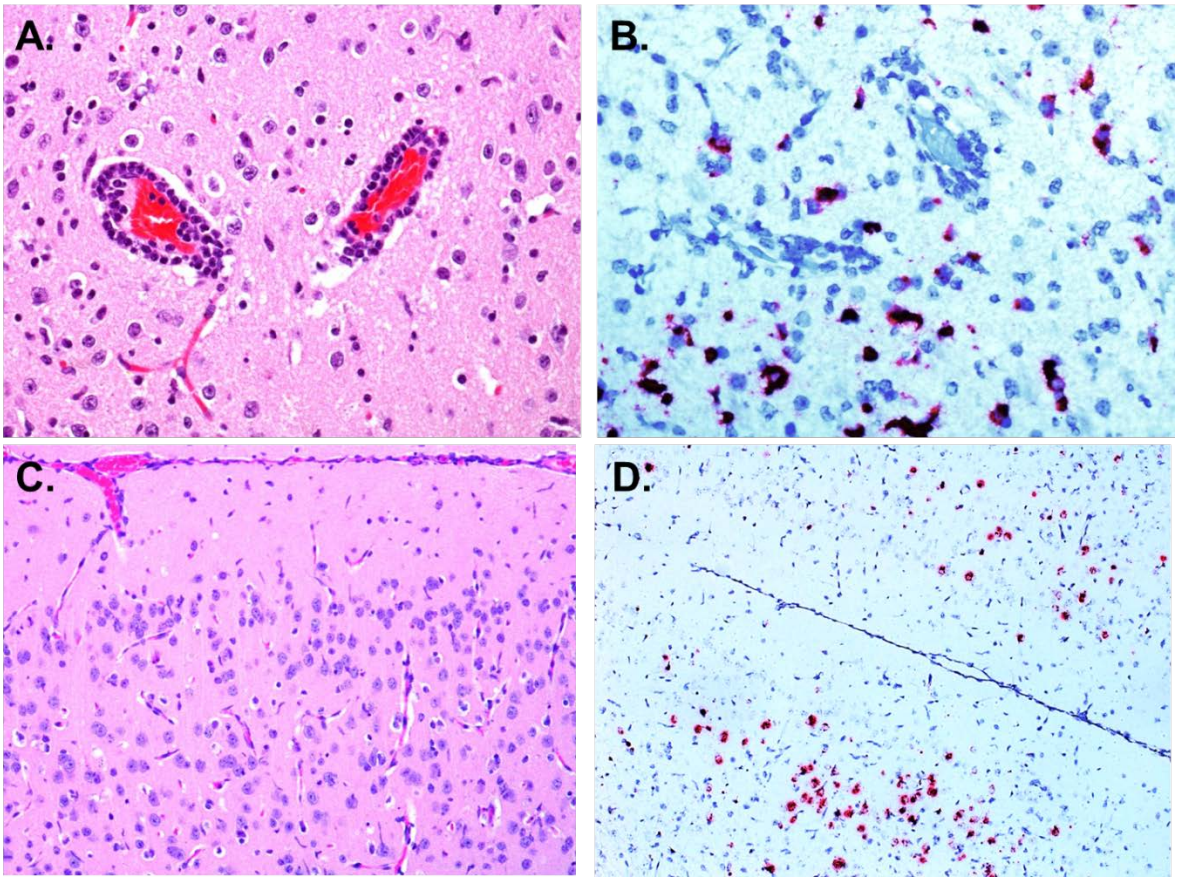

Fig 3. Histologic and ISH Findings in the Cerebrum of ZIKV Infected WT Mice Treated with an IFNAR1-Blocking mAb. (A-B) The cerebrum of a mouse exposed to ZIKV IP that succumbed on day 7 PI. Representative hematoxylin and eosin staining showed perivascular cuffing of vessels with mononuclear cells and few neutrophils. Within the adjacent, vacuolated neuropil there are few neutrophils admixed with scattered necrotic cellular debris and activated microglial cells (A); 400X. Representative ISH staining demonstrating that ZIKV RNA is scattered throughout the same area (B). (C-D) The cerebrum of a mouse exposed to ZIKV IP that was euthanized on day 11 PI. Representative hematoxylin and eosin staining showed the neuropil contains scattered necrotic cellular debris and activated microglia (C); 200X. Representative ISH staining demonstrating that ZIKV RNA is detected throughout the same region (D); 100X.

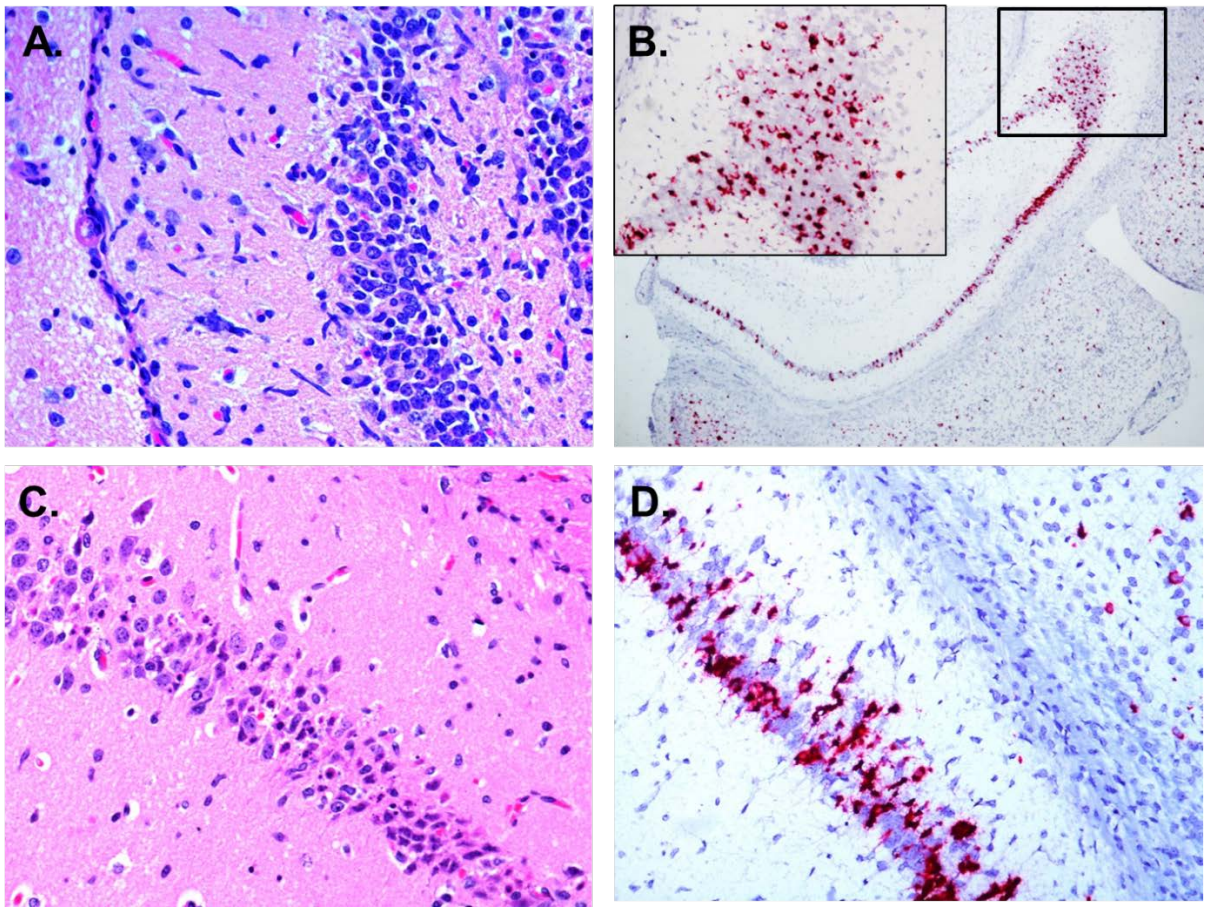

Fig 4. Histologic and ISH Findings in the Hippocampus of ZIKV Infected WT Mice Treated with an IFNAR1-Blocking mAb. (A) The hippocampus of a mouse exposed to ZIKV IP that was euthanized on day 11 PI. Representative hematoxylin and eosin staining showed neuropil vacuolation (edema), microgliosis, and necrotic cellular debris; 400X. (B) The hippocampus of a mouse exposed to ZIKV IP that was euthanized on day 7 PI. The representative ISH staining demonstrates massive ZIKV infection of the brain; 100X. (C-D) The hippocampus of a mouse exposed to ZIKV IP that was euthanized on day 7 PI. The representative hematoxylin and eosin staining demonstrates that pyramidal neurons are often necrotic and the adjacent vacuolated neuropil contains necrotic scattered cellular debris (C); 400X. Representative ISH staining demonstrating that ZIKV RNA is detected in the same region (D); 200X.

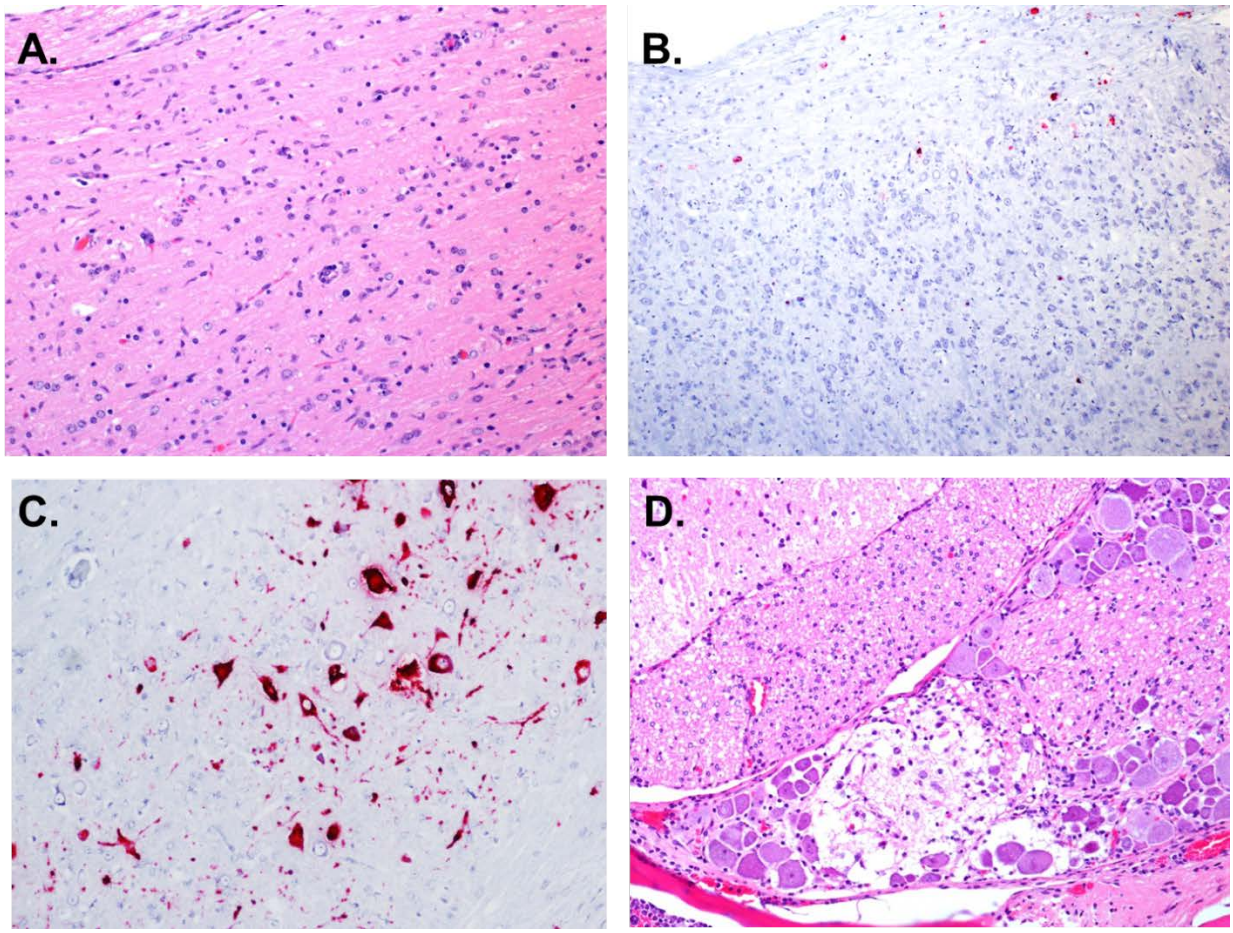

Fig 5. Histologic and ISH Findings in the spinal cord of ZIKV Infected WT Mice Treated with an IFNAR1-Blocking mAb. (A-B) The spinal cord of a mouse that was exposed to ZIKV SC and euthanized on day 8 PI. Representative hematoxylin and eosin staining showed there is scattered necrotic cellular debris, gliosis, and perivascular cuffing (A); 200X. Representative ISH staining demonstrating that ZIKV RNA is detected throughout the same region (B); 100X. (C) ISH staining demonstrating massive ZIKV infection in the spinal cord of a mouse that was exposed to ZIKV IP and was euthanized on day 7 PI. (D) Hematoxylin and eosin staining of spinal ganglion demonstrates a focal area of necrosis with adjacent gliosis and few infiltrating neutrophils in a mouse exposed to ZIKV IP that succumbed on day 7 PI.

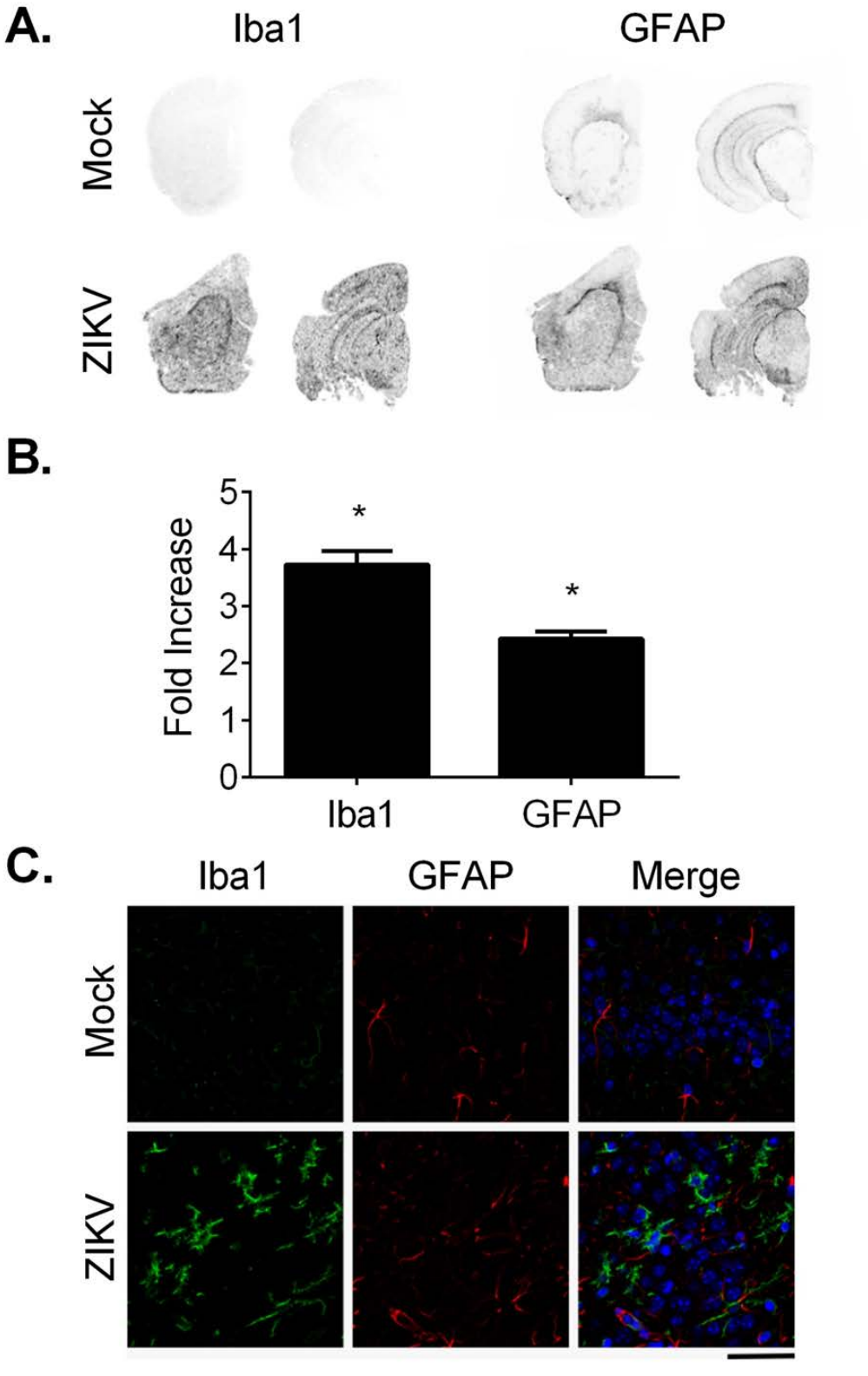
A.
Iba1
GFAP
Mock
ZIKV
B.
Fold Increase
5
4
3
2
1
0
*
*
Iba1
GFAP
C.
Iba1
GFAP
Merge
Mock
ZIKV

Fig 6. Iba1 and GFAP are increased in the brains of ZIKV infected mice. (A-B) Brain sections from mice treated with IFNAR1-blocking mAb and infected with ZIKV or mock infected with PBS were imaged and analyzed by infrared imaging. Representative images showed increased Iba1 and GFAP staining in brain sections from ZIKV-infected mice compared to PBS-inoculated mice. (B) The average infrared intensity was significantly increased in ZIKV-infected mice compared to PBS-inoculated mice for both Iba1 (PBS: 0.9929 ± 0.1614, n=5; ZIKV: 3.725 ± 0.2415, n=10; *p < 0.0001, t-test) and GFAP (PBS: 1.000 ± 0.1022, n=5; ZIKV: 2.429 ± 0.1252, n=10; *p < 0.0001, t-test). (C) Representative images of Iba1 and GFAP immunofluorescent labeling of Iba1 (Green) and GFAP (red) in brain sections of mock- or ZIKV-infected mice. Scale bar represents 50 μm.

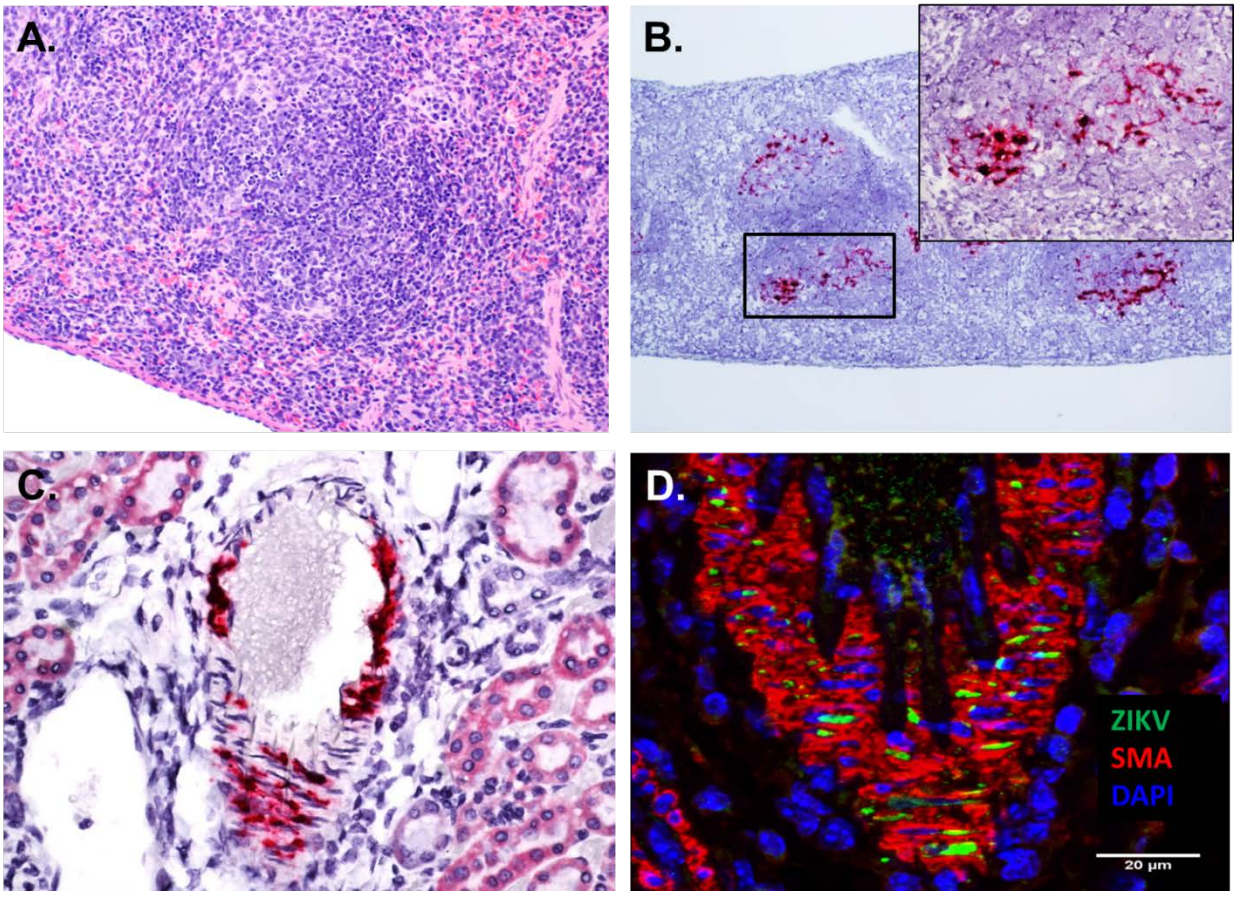

Fig 7. Histologic, ISH, and IFA Findings in the Spleen and Kidney of ZIKV Infected WT Mice Treated with an IFNAR1-Blocking mAb. (A) Representative hematoxylin and eosin staining showed lymphocytolysis within the follicles in the spleen of a mouse exposed to ZIKV IP that was euthanized on day 11 PI; 200X. (B) Representative ISH staining demonstrating that multifocally, ZIKV RNA is detected in the lymphoid follicles in the spleen of a mouse exposed to ZIKV IP that was euthanized on day 11 PI; 100X. (C) Representative ISH staining demonstrating that ZIKV RNA is detected in the muscle cells of a blood vessel in the kidney of a mouse exposed to ZIKV IP that succumbed on day 7 PI; 400X. (D) IFA confirmed the presence of ZIKV in the smooth muscle (SMA) of a blood vessel in the kidney of a mouse exposed to ZIKV IP that succumbed on day 7 PI.

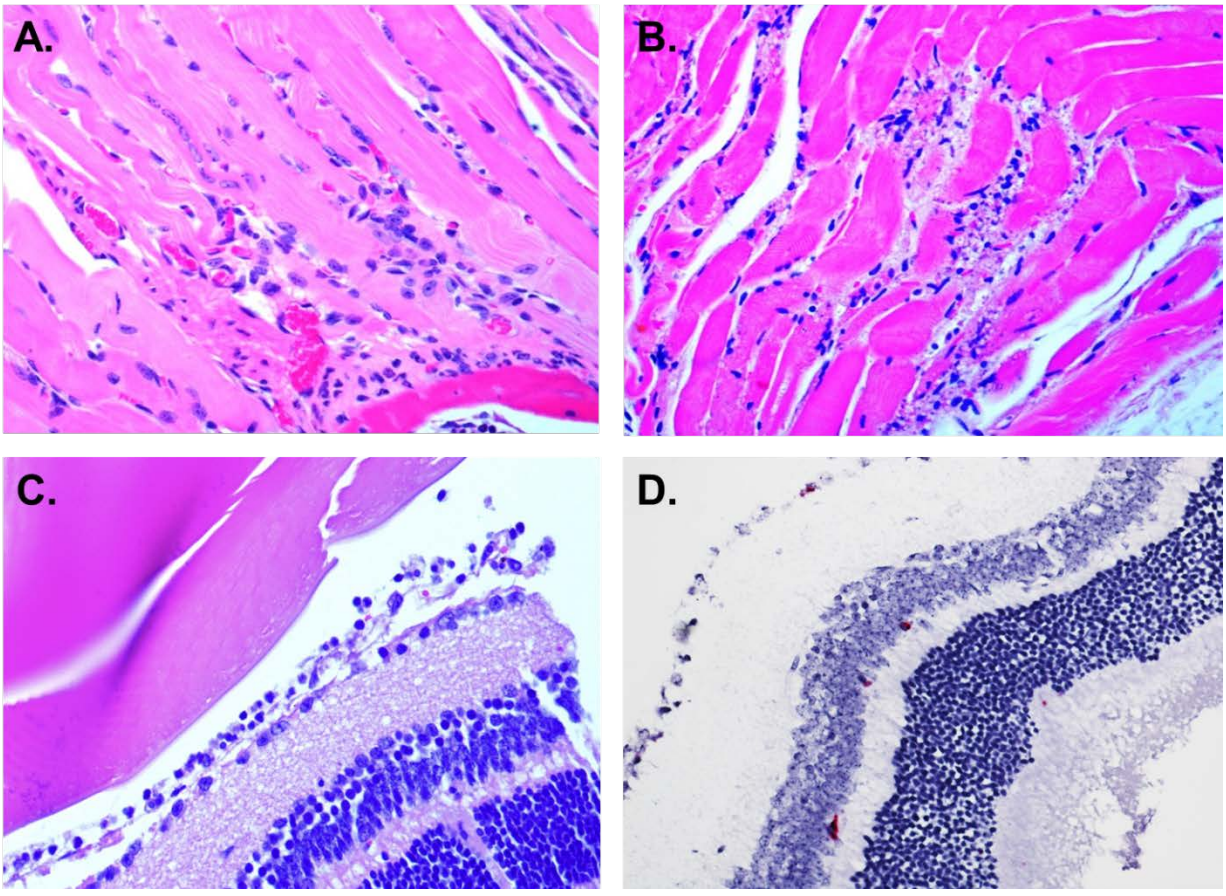

Fig 8. Histologic and ISH Findings in the Skeletal Muscle and Eye of ZIKV Infected WT Mice Treated with an IFNAR1-Blocking mAb. (A) Hematoxylin and eosin staining showed myocyte degeneration, inflammation, and nuclear rowing in the vertebral column skeletal muscle of a mouse exposed to ZIKV IP that was euthanized on day 12 PI; 400X. (B) Hematoxylin and eosin staining showed multifocal myocyte degeneration and inflammation in the skeletal muscle of the head of a mouse exposed to ZIKV IP that succumbed on day 11 PI; 400X. (C) Hematoxylin and eosin staining showed inflammatory infiltrates between the retina and lens of a mouse that was exposed to ZIKV IP and was euthanized on day 8 PI; 400X. (D) ISH staining identified only a few ZIKV positive ganglion cells and inner nuclear layers of the eye of a mouse that was exposed to ZIKV IP and was euthanized on day 7 PI; 400X.

REFERENCES

1. Gatherer D, Kohl A (2016) Zika virus: a previously slow pandemic spreads rapidly through the Americas. J Gen Virol 97: 269-273.
2. Pierson TC, Diamond, M.S. (2013) Flaviviruses. In: Knipe DM, Howley, P.M., editor. Fields Virology. 6th ed. Philadelphia, PA: Lippincott Williams & Wilkins. pp. 747-794.
3. Dick GW (1952) Zika virus. II. Pathogenicity and physical properties. Trans R Soc Trop Med Hyg 46: 521-534.
4. Dick GW, Kitchen SF, Haddow AJ (1952) Zika virus. I. Isolations and serological specificity. Trans R Soc Trop Med Hyg 46: 509-520.
5. Duffy MR, Chen TH, Hancock WT, Powers AM, Kool JL, et al. (2009) Zika virus outbreak on Yap Island, Federated States of Micronesia. N Engl J Med 360: 2536-2543.
6. Hayes EB (2009) Zika virus outside Africa. Emerg Infect Dis 15: 1347-1350.
7. Lanciotti RS, Kosoy OL, Laven JJ, Velez JO, Lambert AJ, et al. (2008) Genetic and serologic properties of Zika virus associated with an epidemic, Yap State, Micronesia, 2007. Emerg Infect Dis 14: 1232-1239.
8. Li MI, Wong PS, Ng LC, Tan CH (2012) Oral susceptibility of Singapore Aedes (Stegomyia) aegypti (Linnaeus) to Zika virus. PLoS Negl Trop Dis 6: e1792.
9. Cao-Lormeau VM, Roche C, Teissier A, Robin E, Berry AL, et al. (2014) Zika virus, French polynesia, South pacific, 2013. Emerg Infect Dis 20: 1085-1086.
10. Dupont-Rouzeyrol M, O'Connor O, Calvez E, Daures M, John M, et al. (2015) Co-infection with Zika and dengue viruses in 2 patients, New Caledonia, 2014. Emerg Infect Dis 21: 381-382.

11. Musso D, Cao-Lormeau VM, Gubler DJ (2015) Zika virus: following the path of dengue and chikungunya? Lancet 386: 243-244.
12. Roth A, Mercier A, Lepers C, Hoy D, Duituturaga S, et al. (2014) Concurrent outbreaks of dengue, chikungunya and Zika virus infections - an unprecedented epidemic wave of mosquito-borne viruses in the Pacific 2012-2014. Euro Surveill 19.
13. Campos GS, Bandeira AC, Sardi SI (2015) Zika Virus Outbreak, Bahia, Brazil. Emerg Infect Dis 21: 1885-1886.
14. Zanluca C, Melo VC, Mosimann AL, Santos GI, Santos CN, et al. (2015) First report of autochthonous transmission of Zika virus in Brazil. Mem Inst Oswaldo Cruz 110: 569-572.
15. Hennessey M, Fischer M, Staples JE (2016) Zika Virus Spreads to New Areas - Region of the Americas, May 2015-January 2016. MMWR Morb Mortal Wkly Rep 65: 55-58.
16. Thomas DL, Sharp TM, Torres J, Armstrong PA, Munoz-Jordan J, et al. (2016) Local Transmission of Zika Virus - Puerto Rico, November 23, 2015-January 28, 2016. MMWR Morb Mortal Wkly Rep 65: 154-158.
17. Hills SL, Russell K, Hennessey M, Williams C, Oster AM, et al. (2016) Transmission of Zika Virus Through Sexual Contact with Travelers to Areas of Ongoing Transmission - Continental United States, 2016. MMWR Morb Mortal Wkly Rep 65: 215-216.
18. Maria AT, Maquart M, Makinson A, Flusin O, Segondy M, et al. (2016) Zika virus infections in three travellers returning from South America and the Caribbean respectively, to Montpellier, France, December 2015 to January 2016. Euro Surveill 21.
19. Zammarchi L, Tappe D, Fortuna C, Remoli ME, Gunther S, et al. (2015) Zika virus infection in a traveller returning to Europe from Brazil, March 2015. Euro Surveill 20.
20. Driggers RW, Ho CY, Korhonen EM, Kuivanen S, Jaaskelainen AJ, et al. (2016) Zika Virus Infection with Prolonged Maternal Viremia and Fetal Brain Abnormalities. N Engl J Med 374: 2142-2151.
21. Brasil P, Pereira JP, Jr., Raja Gabaglia C, Damasceno L, Wakimoto M, et al. (2016) Zika Virus Infection in Pregnant Women in Rio de Janeiro - Preliminary Report. N Engl J Med.
22. Mlakar J, Korva M, Tul N, Popovic M, Poljsak-Prijatelj M, et al. (2016) Zika Virus Associated with Microcephaly. N Engl J Med 374: 951-958.
23. Ansar V, Valadi N (2015) Guillain-Barre syndrome. Prim Care 42: 189-193.
24. Cao-Lormeau VM, Blake A, Mons S, Lastere S, Roche C, et al. (2016) Guillain-Barre Syndrome outbreak associated with Zika virus infection in French Polynesia: a case-control study. Lancet.
25. Oehler E, Watrin L, Larre P, Leparc-Goffart I, Lastere S, et al. (2014) Zika virus infection complicated by Guillain-Barre syndrome--case report, French Polynesia, December 2013. Euro Surveill 19.
26. Lazear HM, Diamond MS (2016) Zika Virus: New Clinical Syndromes and its Emergence in the Western Hemisphere. J Virol.
27. Bearcroft WG (1956) Zika virus infection experimentally induced in a human volunteer. Trans R Soc Trop Med Hyg 50: 442-448.
28. Bell TM, Field EJ, Narang HK (1971) Zika virus infection of the central nervous system of mice. Arch Gesamte Virusforsch 35: 183-193.
29. Fagbami AH (1979) Zika virus infections in Nigeria: virological and seroepidemiological investigations in Oyo State. J Hyg (Lond) 83: 213-219.

30. Haddow AJ, Williams MC, Woodall JP, Simpson DI, Goma LK (1964) Twelve Isolations of Zika Virus from Aedes (Stegomyia) Africanus (Theobald) Taken in and above a Uganda Forest. Bull World Health Organ 31: 57-69.
31. Macnamara FN (1954) Zika virus: a report on three cases of human infection during an epidemic of jaundice in Nigeria. Trans R Soc Trop Med Hyg 48: 139-145.
32. McCrae AW, Kirya BG (1982) Yellow fever and Zika virus epizootics and enzootics in Uganda. Trans R Soc Trop Med Hyg 76: 552-562.
33. Reagan RL, Chang SC, Brueckner AL (1955) Electron micrographs of erythrocytes from Swiss albino mice infected with Zika virus. Tex Rep Biol Med 13: 934-938.
34. Way JH, Bowen ET, Platt GS (1976) Comparative studies of some African arboviruses in cell culture and in mice. J Gen Virol 30: 123-130.
35. Weinbren MP, Williams MC (1958) Zika virus: further isolations in the Zika area, and some studies on the strains isolated. Trans R Soc Trop Med Hyg 52: 263-268.
36. Rossi SL, Tesh RB, Azar SR, Muruato AE, Hanley KA, et al. (2016) Characterization of a Novel Murine Model to Study Zika Virus. Am J Trop Med Hyg.
37. Aliota MT, Caine EA, Walker EC, Larkin KE, Camacho E, et al. (2016) Characterization of Lethal Zika Virus Infection in AG129 Mice. PLoS Negl Trop Dis 10: e0004682.
38. Dowall SD, Graham VA, Rayner E, Atkinson B, Hall G, et al. (2016) A Susceptible Mouse Model for Zika Virus Infection. PLoS Negl Trop Dis 10: e0004658.
39. Lazear HM, Govero J, Smith AM, Platt DJ, Fernandez E, et al. (2016) A Mouse Model of Zika Virus Pathogenesis. Cell Host Microbe 19: 720-730.
40. Zmurko J, Marques RE, Schols D, Verbeken E, Kaptein SJ, et al. (2016) The Viral Polymerase Inhibitor 7-Deaza-2'-C-Methyladenosine Is a Potent Inhibitor of In Vitro Zika Virus Replication and Delays Disease Progression in a Robust Mouse Infection Model. PLoS Negl Trop Dis 10: e0004695.
41. Pinto AK, Daffis S, Brien JD, Gainey MD, Yokoyama WM, et al. (2011) A temporal role of type I interferon signaling in CD8+ T cell maturation during acute West Nile virus infection. PLoS Pathog 7: e1002407.
42. Sheehan KC, Lai KS, Dunn GP, Bruce AT, Diamond MS, et al. (2006) Blocking monoclonal antibodies specific for mouse IFN-alpha/beta receptor subunit 1 (IFNAR-1) from mice immunized by in vivo hydrodynamic transfection. J Interferon Cytokine Res 26: 804-819.
43. Teijaro JR, Ng C, Lee AM, Sullivan BM, Sheehan KC, et al. (2013) Persistent LCMV infection is controlled by blockade of type I interferon signaling. Science 340: 207-211.
44. Zhao H, Fernandez E, Dowd KA, Speer SD, Platt DJ, et al. (2016) Structural Basis of Zika Virus-Specific Antibody Protection. Cell 166: 1016-1027.
45. Ladner JT, Wiley MR, Prieto K, Yasuda CY, Nagle E, et al. (2016) Complete Genome Sequences of Five Zika Virus Isolates. Genome Announc 4.
46. Sheehan KC, Lazear HM, Diamond MS, Schreiber RD (2015) Selective Blockade of Interferon-alpha and -beta Reveals Their Non-Redundant Functions in a Mouse Model of West Nile Virus Infection. PLoS One 10: e0128636.
47. Prophet EB, Mills, B., Arrington, J.B., Sobin, L.H. (1992) Laboratory methods for histotechnology. Armed Forces Institute of Pathology, Washington, DC.
48. Eng LF, Ghirnikar RS (1994) GFAP and astrogliosis. Brain Pathol 4: 229-237.
49. Ito D, Imai Y, Ohsawa K, Nakajima K, Fukuuchi Y, et al. (1998) Microglia-specific localisation of a novel calcium binding protein, Iba1. Brain Res Mol Brain Res 57: 1-9.

50. Larocca RA, Abbink P, Peron JP, Zanotto PM, Iampietro MJ, et al. (2016) Vaccine protection against Zika virus from Brazil. Nature 536: 474-478.
51. Hervas-Stubbs S, Perez-Gracia JL, Rouzaut A, Sanmamed MF, Le Bon A, et al. (2011) Direct effects of type I interferons on cells of the immune system. Clin Cancer Res 17: 2619-2627.
52. Le Bon A, Tough DF (2002) Links between innate and adaptive immunity via type I interferon. Curr Opin Immunol 14: 432-436.
53. Roze B, Najioullah F, Signate A, Apetse K, Brouste Y, et al. (2016) Zika virus detection in cerebrospinal fluid from two patients with encephalopathy, Martinique, February 2016. Euro Surveill 21.
54. Carteaux G, Maquart M, Bedet A, Contou D, Brugieres P, et al. (2016) Zika Virus Associated with Meningoencephalitis. N Engl J Med 374: 1595-1596.
55. Mecharles S, Herrmann C, Poullain P, Tran TH, Deschamps N, et al. (2016) Acute myelitis due to Zika virus infection. Lancet 387: 1481.
56. Solomon IH, Milner DA, Folkerth RD (2016) Neuropathology of Zika Virus Infection. J Neuroinfect Dis 7.
57. de Paula Freitas B, de Oliveira Dias JR, Prazeres J, Sacramento GA, Ko AI, et al. (2016) Ocular Findings in Infants With Microcephaly Associated With Presumed Zika Virus Congenital Infection in Salvador, Brazil. JAMA Ophthalmol.
58. Miner JJ, Sene A, Richner JM, Smith AM, Santeford A, et al. (2016) Zika Virus Infection in Mice Causes Panuveitis with Shedding of Virus in Tears. Cell Rep.